INORGANIC
CHEMISTRY
FRONTIERS

INORGANIC CHEMISTRY
FRONTIERS

RESEARCH ARTICLE

Understanding the magnetism of {Fe₂Ln} dimers, step-by-step†

S. G. Baca,[a,b] J. van Leusen,[b] M. Speldrich[b] and P. Kögerler*[b,c]

A magnetochemical comparison between the $\{Fe_4^{III}Ln_2^{III}\}$-type coordination clusters $[Fe_4M_2(OH)_2(N_3)_2 (bdea)_4(O_2CCMe_3)_5(H_2O)]NO_3\cdot2(EtOH)$ (M = Dy, Y) and $[Fe_4M_2(OH)_2(N_3)_2(bdea)_4(O_2CCMe_3)_4(NO_3)_2]\cdot 3(EtOH)$ (M = Gd, Eu; H_2bdea = *N*-butyldiethanolamine), of which $\{Fe_4Dy_2\}$ reveals slow molecular magnetization relaxation up to 6 K, allows assessment of the exchange coupling governing the clusters' multiplet patterns.

Though research on single molecule magnets (SMMs) has reached its peak with most of the underlying spin physics now well understood,[1] the investigation of heterometallic d/f-based SMMs remains a challenging and attractive goal. In lanthanide-containing SMMs exhibiting very large zero-field splitting of the ground state multiplets of the individual 4f ions, the relaxation mechanisms that effectively limit the threshold temperature for the detection of magnetization hysteresis – either of thermal or quantum tunneling origin – are still not completely understood, and these compounds exhibit a surprisingly wide range of relaxation phenomena.[2] All this has prompted an extensive effort to assess the magnetism of polynuclear 4f but also heterometallic d/f coordination clusters,[3] in order to gain a deeper insight into the relaxation pathways. Until now research on polyheterometallic 3d/4f SMMs was mainly focused on Mn/Ln, Co/Ln, and Ni/Ln heterometallic systems.[4] Although some Fe^{III}/Ln^{III} heterometallic coordination clusters have also been reported,[5] only a few of them exhibit slow magnetization relaxation in the absence of a static field, *i.e.* SMM characteristics.[5c,g,i,j,l,n–p] This surprisingly frequent absence of slow magnetization relaxation here might be caused by the stray fields produced by the Fe^{III} spin centers, which apparently increases the probability of relaxation *via* quantum tunneling mechanisms.

At the same time, modeling the thermodynamic magnetic properties of more complex 3d/4f spin structures, such as the susceptibility, requires taking into account all microscopic aspects, in particular single ion effects and spin–spin interactions, which frequently lead to over-parameterization issues. In order to minimize the number of magnetically relevant independent fitting parameters, a comparison between nearly isostructural complexes of increasing magnetic complexity allows us to stepwise ascertain the ligand field parameters and exchange energies even of 3d/4f compounds comprising magnetically complex spin centers such as Dy(III).

In this context, we explored the potential of our strategy[6] for using both structure-directing aminoalcohols and carboxylates for the synthesis of heterometallic coordination cluster families based on archetypal triangular $(M/M')_3(\mu_3\text{-O})$ fragments.[7] Here we present the synthesis, structures and magnetic properties of four hexanuclear heterometallic cluster compounds: $[Fe_4Dy_2(OH)_2(N_3)_2(bdea)_4(O_2CCMe_3)_5(H_2O)]NO_3\cdot 2(EtOH)$ (**1**), which exhibits slow magnetization relaxation and non-zero out-of-phase ac susceptibility up to 6 K, and nearly identical analogues comprising diamagnetic Y^{III} ions, $[Fe_4Y_2(OH)_2(N_3)_2(bdea)_4(O_2CCMe_3)_5(H_2O)]NO_3\cdot2(EtOH)$ (**2**), or spin-only Gd^{III} ions, $[Fe_4Gd_2(OH)_2(N_3)_2(bdea)_4(O_2CCMe_3)_4(NO_3)_2]\cdot3(EtOH)$ (**3**). Another compound virtually isostructural to **3** but incorporating Eu^{III} ions, $[Fe_4Eu_2(OH)_2(N_3)_2(bdea)_4(O_2CCMe_3)_4(NO_3)_2]\cdot3(EtOH)$ (**4**), has also been prepared.

The reaction of the μ-oxo-centered trinuclear iron pivalate with sodium azide and lanthanide(III)/yttrium(III) nitrate in the presence of *N*-butyldiethanolamine (H_2bdea) in a 2:1:1:2 ratio in ethanol solution produced crystals of **1–4** in relatively high yields (53%, 21%, 40% and 46% based on Fe, respectively). All compounds remain thermally stable up to *ca.* 200 °C. Single-crystal X-ray diffraction analysis‡ reveals that all

aInstitute of Applied Physics, Academy of Sciences of Moldova, 5 Academiei str., Chisinau, MD-2028, Moldova
bInstitute of Inorganic Chemistry, RWTH Aachen University, Landoltweg 1, D-52074 Aachen, Germany. E-mail: paul.koegerler@ac.rwth-aachen.de
cPeter Grünberg Institute, PGI-6, Research Centre Jülich, D-52425 Jülich, Germany
†Electronic supplementary information (ESI) available: Synthesis, characterization, X-ray diffraction, magnetochemical analysis details, additional structural plots and thermal stability data. CCDC 937876, 959015–959017. For ESI and crystallographic data in CIF or other electronic format see DOI: 10.1039/c6qi00095a
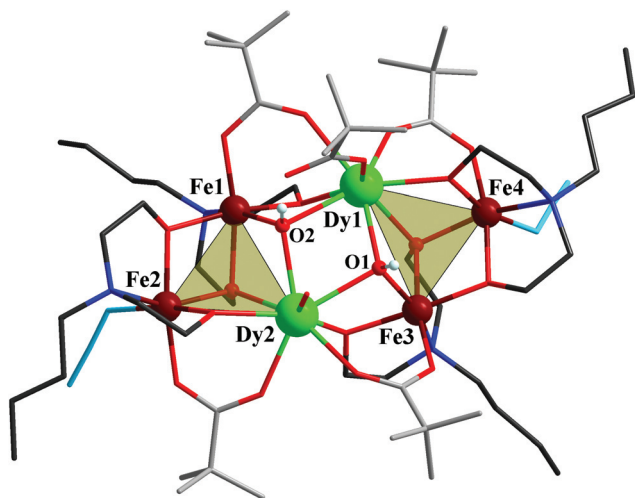
Fig. 1 Structure of the {Fe$_4$Dy$_2$} complex in **1**. Color scheme: O, red; C (carboxylate), light gray; C (bdea), dark gray; N (azide), light blue; N (bdea), dark blue. Only the hydrogen positions of the µ$_3$-OH groups are shown for clarity.

complexes crystallize in the space group $P\bar{1}$ and feature the coordination cluster monocation [Fe$_4$M$_2$(OH)$_2$(N$_3$)$_2$(bdea)$_4$(O$_2$CCMe$_3$)$_5$(H$_2$O)]$^+$ (M = Dy, Y), a nitrate counteranion and two ethanol solvate molecules in **1** and **2**, or the neutral [Fe$_4$M$_2$(OH)$_2$(N$_3$)$_2$(bdea)$_4$(O$_2$CCMe$_3$)$_4$(NO$_3$)$_2$] (M = Gd, Eu) cluster and three ethanol solvates in **3** and **4**. As complexes **1** and **2** as well as **3** and **4** are isostructural, we limit the structural description to **1** and **3**. The cationic complex in **1** consists of a hexanuclear oxido-linked core fragment of four Fe^{III} and two Dy^{III} ions and can be regarded as two nearly identical Fe$_2$Dy triangles condensed via two µ$_3$-hydroxo groups (Fig. 1), with a Dy···Dy distance of 3.871(6) Å.

Four bridging pivalate groups and four doubly deprotonated N-butyldiethanolamine ligands additionally bridge the Fe$_2$Dy triangles [Dy···Fe, 3.392(12) and 3.404(11) Å] and the metal sites within each triangle motif [Fe···Fe, 3.169(15)–3.172(17) Å; Fe···Dy, 3.450(12)–3.542(12) Å]. The central [Fe$_4$Dy$_2$(µ-O)$_{10}$] fragment can alternatively be decomposed into four edge-sharing [M$_2$M′(µ$_3$-O)] triangles: Fe1Fe2Dy2, Dy1Dy2Fe1, Dy1Dy2Fe3, and Fe3Fe4Dy1. Two (end-on) azide ligands (to Fe2/Fe4), one monodentate carboxylate and a water molecule (to Dy1/Dy2) complete the metal coordination spheres. Each N-butyldiethanolamine group links two Fe^{III} and two Dy^{III} atoms: two polyalcohol residues act as hexadentate ligands via

one N atom and µ$_3$-O and µ$_2$-O atoms and the remaining two bdea^{2-} act as pentadentate ligands via one N atom and two µ$_2$-O linkages. All Fe(III) ions adopt distorted octahedral environments: Fe1 and Fe3 are NO$_5$ coordinated by a µ$_3$-OH group [Fe–(µ$_3$-O), 1.943(5)/1.969(5) Å], a carboxylate oxygen [Fe–O$_{carb}$, 1.967(6)/1.953(6) Å] as well as three alkoxy oxygen atoms (one µ$_3$-O and two µ$_2$-O) from two bdea^{2-} groups [Fe–O$_{alk}$, 1.968(5)–2.069(5) Å] and a nitrogen atom from one polyalcoholamine [Fe–N, 2.218(7)/2.196(7) Å]; Fe2 and Fe4 are N$_2$O$_4$ coordinated by a carboxylate oxygen atom [Fe–O$_{carb}$, 2.027(6)/2.046(6) Å], three alkoxy oxygen atoms (one µ$_3$-O, two µ$_2$-O) of two bdea^{2-} groups [Fe–O$_{alk}$, 1.949(5)–2.055(5) Å], a bdea^{2-}-N atom [Fe–N$_{alk}$, 2.212(7)/2.215(6) Å] and an azide-N atom [Fe–N$_{azide}$, 1.992(8)/1.990(8) Å]. Both Dy^{III} ions are eight-coordinated: two µ$_3$-OH$^-$ groups, two oxygen atoms from two carboxylates, two alkoxy µ$_2$-O and one µ$_3$-O atoms from two bdea^{2-}; Dy1 additionally binds to a monodentate pivalate, Dy2 to H$_2$O [Dy–O, 2.304(5)–2.364(5) Å]. The coordinated water molecule and monodentate pivalate as well as the outer-sphere nitrate anion and two solvate ethanol molecules engage in extensive intra- and intermolecular hydrogen bonding in **1**. In particular, one of the OH$^-$ groups forms a strong intramolecular O–H···O hydrogen bond [2.608(8) Å] with the uncoordinated carboxylate oxygen (O2···O4), whereas the second hydroxide forms an intermolecular O–H···O hydrogen bond [2.777(8) Å] with the nitrate anion (O1···O22, see Fig. S2†).

Very similar to **1**, the charge-neutral coordination cluster in **3** also consists of a hexanuclear oxido-linked core fragment of four Fe^{III} and two Gd^{III} ions or two nearly identical Fe$_2$Gd triangles bridged by two µ$_3$-OH groups [Gd···Gd, 4.053(1) Å, Fig. S5†]. The difference stems from apical ligands coordinated to the two Ln^{III} ions: in **3**, these are two chelated NO$_3^-$ anions vs. monodentate pivalic acid and H$_2$O in **1**. As a result, both Gd^{III} sites are O$_9$-coordinated (Fig. 2); Gd–O, 2.316(8)–2.650(8) Å. The coordination environment of the four Fe^{III} atoms is similar to **1** [NO$_5$ for Fe1 and Fe3, N$_2$O$_4$ for Fe2 and Fe4; Fe–O, 1.965(7)–2.079(7) Å; Fe–N, 1.993(8)–2.254(9) Å].

Magnetochemical analyses of **1**–**4** (Fig. 3) – with the ultimate goal of modeling the magnetically complex {Fe$_4$Dy$_2$}
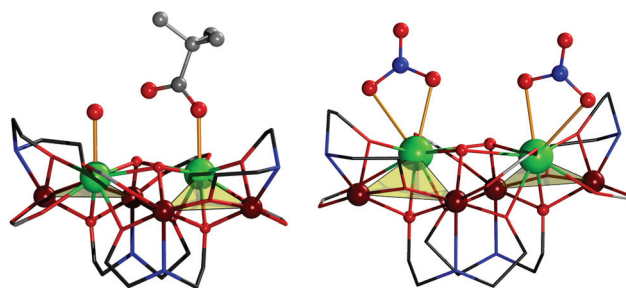
Fig. 2 Comparison of the structure of the {Fe$_4$Dy$_2$} complex in **1** (left) and the {Fe$_4$Gd$_2$} complex in **3** (right), in an approx. perpendicular view to that in Fig. 1. Highlighted are the terminal ligands (H$_2$O and monodentate pivalate in **1**, nitrate in **3**) resulting in eight- and nine-coordinated lanthanide centers. All terminal organic residues, azide and hydrogen omitted for clarity.

1072 | *Inorg. Chem. Front.*, 2016, **3**, 1071–1075

This journal is © the Partner Organisations 2016
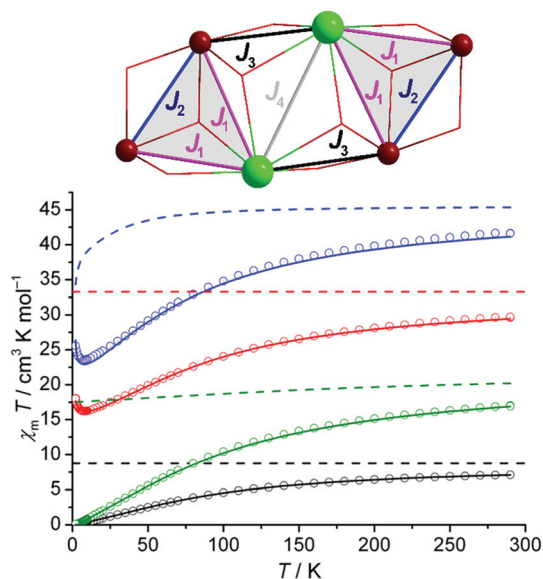
Fig. 3 Top: Coupling scheme for the $\{Fe_4Ln_2\}$ core structure with four exchange constants (J_{1-4}). Bottom: Temperature dependence of χT for **1** (Dy, blue), **2** (Y, black), **3** (Gd, red), and **4** (Eu, green) at 0.1 Tesla. Open circles: experimental data, lines: least-squares fits to the employed model Hamiltonian (see text). Dashed lines: sum of (uncoupled) single ion effects of each $\{Fe_4Ln_2\}$ entity.

species **1** – employed the computational framework CONDON that implements a 'full model' Hamiltonian and thus accounts for all microscopic aspects necessary to model the complex 3d–4f spin structure,[8] in particular the relevant single-ion effects and coupling interactions (see the ESI† for computational details). To quantify these effects, we analyzed the magnetic susceptibility data considering ligand-field effects, spin–orbit coupling, and external magnetic field. Standard values are employed for spectroscopic parameters (*e.g.* Racah energies *B* and *C* or spin–orbit coupling energies). CONDON alternatively implements an effective isotropic spin model that is used for comparison where applicable. Note that the presence of at least three different exchange pathways (all mediated by μ_3-O bridges) precludes the unambiguous direct determination of their associated exchange energies (J_1, J_2, J_3, J_4, or the molecular field parameter λ_{mf}; see coupling scheme) based on $\chi_m(B,T)$ data. Furthermore, the computational requirements for a full model of the hexanuclear $\{Fe_4Ln_2\}$ cluster mandate a simplification to the coupling scheme that is herein divided into two identical $\{Fe_2Ln\}$ triangles (see Fig. 1), the interaction of which is accounted for by a molecular field term. To address these issues the following strategy was employed: we start with the magnetically simplest system $\{Fe_4Y_2\}$ containing diamagnetic Y^{III} to extract the parameters of the Fe^{III} centers which are adopted for all other systems. Next, $\{Fe_4Gd_2\}$ is analyzed as a purely isotropic spin system; these results are compared to full-model calculations based on the two-triangle coupling scheme, in order to validate the latter. Finally, full-model calculations are applied to $\{Fe_4Dy_2\}$.

$\{Fe_4Eu_2\}$ serves as an additional reference point for this approach.

Given the nearly identical geometries, the nearest-neighbor Fe–Fe coupling (J_2) is assumed to vary minimally between **1–4** and can be directly determined from the $\{Fe_4Y_2\}$ species (**2**). Based on the angular overlap model, implemented and parameterized in the program wxJFinder,[7b] these variations should not exceed ±10% for the individual Fe–O(H)–Fe exchange pathway geometries in **1–4**. Here, any inter-triangle Fe···Fe exchange coupling (which would involve extended –O–Y–O– exchange pathways) can be neglected and the Heisenberg-type intra-molecular exchange interaction pattern ($H_{ex} = -2J_2 S_1 \cdot S_2$) is simplified to that of a spin dimer. The tetragonally distorted FeO_6 coordination environments in **1–4** are best described as D_{4h} symmetric; for this assumption the Fe^{III} ligand field parameters derived from a least-squares fit for **2** are $B_0^2 = -3500$ cm^{-1}, $B_0^4 = 24\,000$ cm^{-1}, and $B_4^4 = 19\,000$ cm^{-1} (in Wybourne notation) and $J_2 = -6.5$ cm^{-1} ($SQ = 1.0\%$; Fig. 3). These B_q^k values are used as constants in the fitting procedures of **1**, **3**, and **4**. As is evident from the susceptibility temperature dependence (at 0.1 Tesla; Fig. S9†) with a maximum at 55 K and a minimum at 5 K, a small paramagnetic impurity is present and it can also be quantified ($\rho = 0.2\%$). Analyzing **2** as a purely isotropic spin system ($g_{eff} = g_S = 2.0$) results in a slightly worse fit but yields the same J_2 value of -6.5 cm^{-1} ($SQ = 1.8\%$, $\rho = 0.25\%$; Fig. S10†).

Next, we swap diamagnetic Y^{III} for spin-only Gd^{III} centers, *i.e.* moving from **2** to **3**. The low-field χT curve of **3** decreases from 29.6 cm^3 K mol^{-1} and reaches a minimum of around 16.6 cm^3 K mol^{-1} at 8.0 K. Approximating $\{Fe_4Gd_2\}$ as an isotropic spin system, a least-squares fit to a Heisenberg-type Hamiltonian (see coupling scheme, Fig. 3) yields $J_1 = -(0.38 \pm 0.12)$ cm^{-1}, $J_2 = -(6.5 \pm 0.1)$ cm^{-1}, $J_3 = +(0.20 \pm 0.06)$ cm^{-1} and $J_4 = +(0.03 \pm 0.01)$ cm^{-1} ($SQ = 1.2\%$; see the ESI† for correlation analysis). We note that the converged J_2 value is identical to that for **2**, as expected for the nearly identical exchange pathway geometries. The weak Gd···Gd contact (J_4) is found to be approx. one order of magnitude smaller than the Gd···Fe contacts; weak ferromagnetic interactions are also documented for μ_3-hydroxo-bridged Fe···Gd[9a] and Gd···Gd[9b] examples.

As mentioned above, modeling the Fe^{III} and Gd^{III} centers in $\{Fe_4Gd_2\}$ with their full single-ion effects mandates restrictions to the exchange coupling scheme in the model Hamiltonian: the $\{Fe_4Gd_2\}$ cluster is described as a dimer of triangles, where all inter-triangle exchange interactions are represented by the molecular field approximation $\chi^{-1} = \chi'^{-1} - \lambda_{mf}$, where χ' represents the susceptibility contribution of the two uncoupled $\{Fe_2Gd\}$ triangles. This model then yields $B_0^2 = -200$ cm^{-1}, $B_0^4 = -1900$ cm^{-1}, and $B_0^6 = 205$ cm^{-1} for Gd^{3+} and $J_1 = -0.42$ cm^{-1}, $J_2 = -6.5$ cm^{-1} and $\lambda_{mf} = +0.042$ mol cm^{-3} ($SQ = 1.9\%$). Both models for **3** are in excellent agreement, see Fig. S11,† with identical values for J_2 and ferromagnetic inter-triangle coupling (*i.e.* $\lambda_{mf} > 0$).

The $\{Fe_4Eu_2\}$ species (**4**) with its nearly temperature-independent paramagnetic Eu^{III} centers ($m_j = 0$, see Fig. S9†) further corroborates that the J_2 value is nearly independent of

the lanthanide in the $\{Fe_4Ln_2\}$ family. The χ vs. T curve (0.1 Tesla) shows a maximum at 55 K and a minimum at 5 K, i.e. the same as those for **2**. Thus, in a first-order approximation we adopted the coupling scheme for **2**, augmented by the additive contributions of the two Eu^{III} centers. A least-squares fit ($SQ = 1.0\%$) then yields $B_0^2 = -150$ cm^{-1}, $B_0^4 = -1940$ cm^{-1}, $B_0^6 = 208$ cm^{-1} (lf parameters for Eu^{III}) and confirms $J_2 = -6.7$ cm^{-1}.

The magnetism of the $\{Fe_4Dy_2\}$ species (**1**), with the Dy^{III} ions in a non-cubic coordination environment, is strongly dependent on both the single-ion effects, in particular the thermal population of higher Dy^{III} multiplet states, and the $Fe\cdots Fe$ and $Fe\cdots Dy$ interactions. The increase in χT with decreasing temperatures below 8 K that is also observed for **2** is caused by very weak ferromagnetic inter-triangle interactions. Akin to **2**, the $\{Fe_4Dy_2\}$ unit is modeled as a dimer of identical isosceles triangles, in order to allow the usage of the Russell–Saunders ground term for each Dy^{III} ion and Fe^{III} ion (note that the full $\{Fe_4Dy_2\}$ system would require 3.2 TByte random access memory for matrix diagonalization). The assumption of D_{4d}-symmetric $Dy^{III}O_8$ environments in **1** was found to be an adequate approximation, a less-symmetric ligand field (correspondingly parameterized by a higher number of independent ligand field parameters) did not significantly increase the fitting quality. As for **2**, intra-triangle exchange interactions are described by Heisenberg coupling; all inter-triangle interactions were modeled via the molecular field approximation. A least-squares fit ($SQ = 1.6\%$) results in $B_0^2 = -300$ cm^{-1}, $B_0^4 = -1850$ cm^{-1}, and $B_0^6 = 210$ cm^{-1} for Dy^{III} and $J_1 = -0.48$ cm^{-1}, $J_2 = -6.7$ cm^{-1}, and $\lambda_{mf} = +0.075$ mol cm^{-3}. Note that J_2 converges very close to the corresponding values for **2–4** and that the $Fe\cdots Dy$ exchange energy (J_1) as expected is very similar to the $Fe\cdots Gd$ exchange in **2**. The derived lf parameters for Dy^{III} correspond to a zero-field splitting of the free-ion $j = 15/2$ ground state multiplet into m_j levels, where the lowest states with $m_j = \pm 11/2$ are 7.9 cm^{-1} below the next-highest $m_j = \pm 9/2$ states (Fig. 4a). The energetic

separation to the $m_j = \pm 1/2$ states, relevant for thermal magnetization relaxation processes, is 240.4 cm^{-1}.

Therefore, alternating-current magnetic susceptibility measurements with no dc bias were analyzed in order to determine if these splitting patterns lead to an effective slowing-down of the relaxation of the magnetization upon an external field change. Frequency-dependent peaks are observed in the out-of-phase response and indicate that $\{Fe_4Dy_2\}$ exhibits single-molecule characteristics up to 6 K, although this is close to the thermal quantum regime (Fig. S12 and S13†). The corresponding real (in-phase) χ' and the imaginary (out-of-phase) components χ'' were fitted to a Cole–Cole equation (Fig. 4b).[9c] The resulting average relaxation times of the magnetization, τ, allow the parameterization of common relaxation process types. The observed spread in α (0.03–0.24) indicates several relaxation pathways, and we determined that a combined Orbach–Raman relaxation, $\tau = 1/[\tau_0^{-1} \exp(-\Delta E/k_B T) + CT^n]$, allows for a more adequate determination of relaxation parameters (Fig. S14†). This results in an attempt time $\tau_0 = (1.01 \pm 0.89) \times 10^{-7}$ s, an effective relaxation barrier $\Delta E = (18.4 \pm 2.7)$ cm^{-1}, i.e. less than a tenth of the $m_j = \pm 11/2 \cdots \pm 1/2$ splitting, and Raman parameters $n = 6.6 \pm 0.4$ and $C = (0.66 \pm 0.23)$ K^{-n} s^{-1}. We note that the Orbach parameters are similar to previously reported $\{Fe_yDy_z\}$ species.[5n,o] The Raman parameter n is lower than 9, i.e. the value expected for Kramers ions, but such lower values (4–9) have been reported previously and may be due to e.g. optical phonons.[9d]

Conclusions

In conclusion, the four hydroxide-bridged $\{Fe_2M\}$ dimer complexes in **1–4** enable us to analyze their magnetic characteristics in a stepwise, comparative ansatz. In particular, the full magnetochemical analysis of the susceptibility data of the $\{Fe_4Dy_2\}$ species requires exploiting the clusters' close structural relationship in order to avoid over-parametrization issues. The $\{Fe_4Dy_2\}$ compound (**1**) exhibits slow magnetization relaxation, i.e. SMM behavior, which we link to the zero-field splitting of the Dy^{III} ground multiplet. Contrasting all previous work on Fe^{III}/Dy^{III} complexes, herein we were able to also model the Fe–Fe and Fe–Dy coupling energies: antiferromagnetic interactions are dominant, yet weaker inter-triangle interactions appear ferromagnetic. Finally, we cautiously note that our magnetochemical interpretation, based solely on susceptibility data derived from microcrystalline samples, only allows for an assessment within the limitations of the various employed models. Numerous attempts to isolate larger single crystal specimens for single-crystal anisotropy measurements unfortunately remained fruitless.

Fig. 4 (a) Zero-field-split m_j states originating from the $j = 15/2$ ground state multiplet of the Dy^{III} centers in **1**, as derived from the least-squares fit to the susceptibility data. (b) AC susceptibility components for $\{Fe_4Dy_2\}$-type compound **1** for ac frequencies ranging from 1 to 1500 s^{-1}. Experimental data: filled circles, fits to Cole–Cole equation: black lines.

Notes and references

1 D. Gatteschi, R. Sessoli and J. Villain, *Molecular Nanomagnets*, Oxford University Press, New York, 2006.

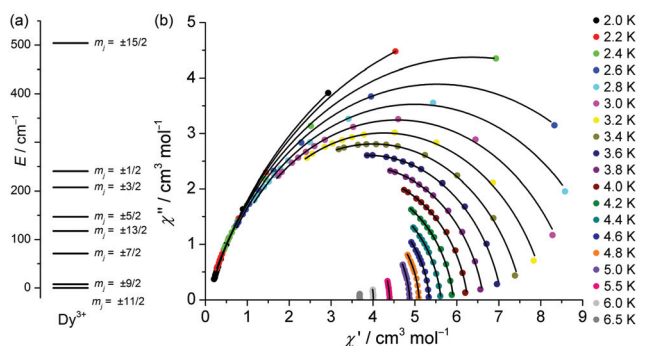**1074** | *Inorg. Chem. Front.*, 2016, **3**, 1071–1075

This journal is © the Partner Organisations 2016

2 (a) M.-E. Boulon, G. Cucinotta, J. Luzon, C. Degl'Innocenti, M. Perfetti, K. Bernot, G. Calvez, A. Caneschi and R. Sessoli, *Angew. Chem., Int. Ed.*, 2013, **52**, 350; (b) F. Moro, D. P. Mills, S. T. Liddle and J. van Slageren, *Angew. Chem., Int. Ed.*, 2013, **52**, 3430; (c) J. Luzon and R. Sessoli, *Dalton Trans.*, 2012, **41**, 13556; (d) F. Tuna, C. A. Smith, M. Bodensteiner, L. Ungur, L. F. Chibotaru, E. J. L. McInnes, R. E. P. Winpenny, D. Collison and R. A. Layfield, *Angew. Chem., Int. Ed.*, 2012, **51**, 6976; (e) S.-Y. Lin, W. Wernsdorfer, L. Ungur, A. K. Powell, Y.-N. Guo, J. Tang, L. Zhao, L. F. Chibotaru and H.-J. Zhang, *Angew. Chem., Int. Ed.*, 2012, **51**, 12767; (f) J. D. Rinehart and J. R. Long, *Chem. Sci.*, 2011, **2**, 2078; (g) N. Magnani, E. Colineau, R. Eloirdi, J.-C. Griveau, R. Caciuffo, S. M. Cornet, I. May, C. A. Sharrad, D. Collison and R. E. P. Winpenny, *Phys. Rev. Lett.*, 2010, **104**, 197202.

3 D. N. Woodruff, R. E. P. Winpenny and R. A. Layfield, *Chem. Rev.*, 2013, **113**, 5110.

4 (a) K. C. Mondal, A. Sundt, Y. Lan, G. E. Kostakis, O. Waldmann, L. Ungur, L. F. Chibotaru, C. E. Anson and A. K. Powell, *Angew. Chem., Int. Ed.*, 2012, **51**, 7550; (b) Y. Zheng, E. Moreno Pineda, M. Helliwell and R. E. P. Winpenny, *Chem. – Eur. J.*, 2012, **18**, 4161; (c) S. K. Langley, L. Ungur, N. F. Chilton, B. Moubaraki, L. F. Chibotaru and K. S. Murray, *Chem. – Eur. J.*, 2011, **17**, 9209; (d) J. Rinck, G. Novitchi, W. van den Heuvel, L. Ungur, Y. Lan, W. Wernsdorfer, C. E. Anson, L. F. Chibotaru and A. K. Powell, *Angew. Chem., Int. Ed.*, 2010, **49**, 7583.

5 (a) A. Baniodeh, Y. Lan, G. Novitchi, V. Mereacre, A. Sukhanov, M. Ferbinteanu, V. Voronkova, Ch. E. Anson and A. K. Powell, *Dalton. Trans.*, 2013, **42**, 8926; (b) Q. Zhou, F. Yang, D. Liu, Y. Peng, G. Li, Z. Shi and S. Feng, *Dalton. Trans.*, 2013, **42**, 1039; (c) S. Schmidt, D. Prodius, V. Mereacre, G. E. Kostakis and A. K. Powell, *Chem. Commun.*, 2013, **49**, 1696; (d) S. Schmidt, D. Prodius, G. Novitchi, V. Mereacre, G. E. Kostakis and A. K. Powell, *Chem. Commun.*, 2012, **48**, 9825; (e) A. Baniodeh, I. J. Hewitt, V. Mereacre, Y. Lan, G. Novitchi, C. E. Anson and A. K. Powell, *Dalton Trans.*, 2011, **40**, 4080; (f) V. Mereacre, D. Prodius, Y. Lan, K. Turta, C. E. Anson and A. K. Powell, *Chem. – Eur. J.*, 2011, **17**, 123; (g) S. Nayak, O. Roubeau, S. J. Teat, C. M. Beavers, P. Gamez and J. Reedijk, *Inorg. Chem.*, 2010, **49**, 216; (h) D. Schray, G. Abbas, Y. Lan, V. Mereacre, A. Sundt, J. Dreiser, O. Waldmann, G. E. Kostakis, C. E. Anson and A. K. Powell, *Angew. Chem., Int. Ed.*, 2010, **49**, 5185; (i) Y.–F. Zeng, G.-C. Xu, X. Hu, Z. Chen, X.-H. Bu, S. Gao and E. C. Sanudo, *Inorg. Chem.*, 2010, **49**, 9734; (j) G. Abbas, Y. Lan, V. Mereacre, W. Wernsdorfer, R. Clerac, G. Buth, M. T. Sougrati, F. Grandjean, G. J. Long, C. E. Anson and A. K. Powell, *Inorg. Chem.*, 2009, **48**, 9345; (k) M. N. Akhtar, V. Mereacre, G. Novitchi, J. P. Tuchagues, C. E. Anson and A. K. Powell, *Chem. – Eur. J.*, 2009, **15**, 7278; (l) J. Bartolome, G. Filoti, V. Kuncser, G. Schinteie, V. Mereacre, C. E. Anson, A. K. Powell, D. Prodius and C. Turta, *Phys. Rev. B: Condens. Matter*, 2009, **80**, 014430; (m) F. Pointillart, K. Bernot, R. Sessoli and D. Gatteschi, *Chem. – Eur. J.*, 2007, **13**, 1602; (n) M. Ferbinteanu, T. Kajiwara, K. Y. Choi, H. Nojiri, A. Nakamoto, N. Kojima, F. Cimpoesu, Y. Fujimura, S. Takaishi and M. Yamashita, *J. Am. Chem. Soc.*, 2006, **128**, 9008; (o) M. Murugesu, A. Mishra, W. Wernsdorfer, K. A. Abboud and G. Christou, *Polyhedron*, 2006, **25**, 613; (p) S. Chen, V. Mereacre, C. E. Anson and A. K. Powell, *Dalton Trans.*, 2016, **45**, 98.

6 (a) I. L. Malaestean, M. Kutluca, M. Speldrich, A. Ellern and P. Kögerler, *Inorg. Chim. Acta*, 2012, **380**, 72; (b) I. L. Malaestean, M. Speldrich, A. Ellern, S. G. Baca and P. Kögerler, *Dalton Trans.*, 2011, **40**, 331; (c) I. L. Malaestean, M. Speldrich, A. Ellern, S. G. Baca and P. Kögerler, *Polyhedron*, 2010, **29**, 1990; (d) S. G. Baca, M. Speldrich, J. van Leusen, A. Ellern and P. Kögerler, *Dalton Trans.*, 2015, **44**, 7777.

7 (a) G. M. Dulcevscaia, I. G. Filippova, M. Speldrich, J. Leusen, V. C. Kravtsov, S. G. Baca, P. Kögerler, S.-X. Liu and S. Decurtins, *Inorg. Chem.*, 2012, **51**, 5110; (b) S. G. Baca, T. Secker, A. Mikosch, M. Speldrich, J. van Leusen, A. Ellern and P. Kögerler, *Inorg. Chem.*, 2013, **52**, 4154.

8 (a) M. Speldrich, H. Schilder, H. Lueken and P. Kögerler, *Isr. J. Chem.*, 2011, **51**, 215; (b) J. van Leusen, M. Speldrich, H. Schilder and P. Kögerler, *Coord. Chem. Rev.*, 2015, **289–290**, 137.

9 (a) S. Mukherjee, M. R. Daniels, R. Bagai, K. A. Abboud, G. Christou and C. Lampropoulos, *Polyhedron*, 2010, **29**, 54; (b) T. S. Hatscher and W. Urland, *Angew. Chem., Int. Ed.*, 2003, **42**, 2862; (c) K. S. Cole and R. H. Cole, *J. Chem. Phys.*, 1941, **9**, 341; (d) K. Shrivastava, *Phys. Status Solidi B*, 1983, **117**, 437.

This journal is © the Partner Organisations 2016

Inorg. Chem. Front., 2016, **3**, 1071–1075 | **1075**